Summer Undergraduate Research Experience Project Report

Investigating Topological Phases of Matter

Ruaidhrí Campion
Supervised by Prof. Mark Mitchison

26^{th} August 2022

Contents

1 Abstract

In this project, the Qi-Wu-Zhang (QWZ) model [1] is studied.

The energy eigenvalues of the QWZ Hamiltonian matrix are calculated for various values of the energy splitting, and the correspondence between energy and bulk/edge state is shown for both trivial and non-trivial topology.

An impurity is introduced into the system, and the decoherence over time is calculated for a variety of system parameters (system size, energy splitting, temperature, impurity location, coupling strength). The effect of varying these parameters is demonstrated by plotting the decoherence magnitude and phase as a function of time for each set of parameters.

2 Introduction

2.1 QWZ Model

The QWZ model [1] consists of a 2D grid of lattice sites capable of hosting a fermion with two flavour states. For a system of size $L_x \times L_y$, on-site energy ω_0, flavour energy splitting m, and tunneling amplitudes t_X, t_Y, the Hamiltonian $\hat{H}_0 = \hat{H}_m + \hat{H}_X + \hat{H}_Y$ is given by [2]

$$\begin{aligned} \hat{H}_m &= \sum_{x=1}^{L_x}\sum_{y=1}^{L_y} \hat{\mathbf{a}}^\dagger_{x,y} \cdot (\omega_0 \mathbb{I} + m\sigma_z) \cdot \hat{\mathbf{a}}_{x,y}, \\ \hat{H}_X &= \frac{t_X}{2}\sum_{x=1}^{L_x}\sum_{y=1}^{L_y} \hat{\mathbf{a}}^\dagger_{x+1,y} \cdot (\sigma_z + i\sigma_y) \cdot \hat{\mathbf{a}}_{x,y} + \text{h.c.}, \\ \hat{H}_Y &= \frac{t_Y}{2}\sum_{x=1}^{L_x}\sum_{y=1}^{L_y} \hat{\mathbf{a}}^\dagger_{x,y+1} \cdot (\sigma_z + i\sigma_x) \cdot \hat{\mathbf{a}}_{x,y} + \text{h.c.}, \end{aligned} \tag{1}$$

where

$$\hat{\mathbf{a}}_{x,y} = \begin{pmatrix} \hat{a}_{x,y,\uparrow} \\ \hat{a}_{x,y,\downarrow} \end{pmatrix}, \qquad \sigma_x = \begin{pmatrix} 0 & 1 \\ 1 & 0 \end{pmatrix}, \qquad \sigma_y = \begin{pmatrix} 0 & -i \\ i & 0 \end{pmatrix}, \qquad \sigma_z = \begin{pmatrix} 1 & 0 \\ 0 & -1 \end{pmatrix}.$$

The eigenvalues of the matrix $\hat{h}_0$, defined as

$$\hat{h}_0 = (h_{i,j}), \qquad \hat{H}_0 = \sum_{i,j=1}^{2L_xL_y} \hat{a}^\dagger_i \, h_{i,j} \, \hat{a}_j, \tag{2}$$

correspond to the energy spectrum of the system, where the sum is over all combinations of coordinates and flavour; a convenient conversion of indices $(x, y, s) \to k$ may be given by

$$k = x + (y-1)L_x + sL_xL_y. \tag{3}$$

The value of m (relative to t_X and t_Y) determines if the system is a topological or trivial insulator (i.e. Figure 1).

2.2 Impurity & Decoherence

An impurity, i.e. an on-site energy shift $\hat{V} = \Delta\, \hat{\mathbf{a}}^\dagger_{x,y} \cdot \hat{\mathbf{a}}_{x,y}$ of coupling strength Δ, can be introduced to the system, resulting in the perturbed Hamiltonian $\hat{H}_1 = \hat{H}_0 + \hat{V}$ and matrix $\hat{h}_1 = \hat{h}_0 + \hat{v}$ defined accordingly. Letting $|\psi(0)\rangle$ be the initial fermion state and defining

$$\begin{aligned} \hat{H} &= |0\rangle\langle 0| \otimes \hat{H}_0 + |1\rangle\langle 1| \hat{H}_1, & |\Psi(0)\rangle &= |+\rangle \otimes |\psi(0)\rangle, \\ |+\rangle &= \frac{1}{\sqrt{2}}(|0\rangle + |1\rangle), & |\Psi(\tau)\rangle &= e^{-i\hat{H}\tau}|\Psi(0)\rangle, \end{aligned}$$

it can be shown that

$$|| \langle + \mid \Psi(\tau) \rangle ||^2 = \frac{1}{2} \left[1 + \mathrm{Re}(\nu(\tau))\right],$$

where the decoherence function $\nu(\tau)$ is defined as [3]

$$\begin{aligned} \nu(\tau) &= \left\langle \psi(0) \,\middle|\, e^{i\hat{H}_0\tau} e^{-i\hat{H}_1\tau} \,\middle|\, \psi(0) \right\rangle \\ &= \det\left[\hat{\mathbb{I}} - \hat{n} + \hat{n} e^{i\hat{h}_0\tau} e^{-i\hat{h}_1\tau}\right], \\ \hat{n} &= \left(1 + e^{\beta(\hat{h}_0 - \mu)}\right)^{-1}. \end{aligned} \tag{4}$$

While Equation 4 can be used to calculate the decoherence at any point in time, it is far more computationally efficient to convert basis to diagonalise $\hat{h}_0$ and $\hat{h}_1$, so that each exponential term in the determinant requires exponentiating $2L_xL_y$ terms as opposed to a $2L_xL_y \times 2L_xL_y$ matrix. Denoting

$$\begin{aligned} \hat{E} &= \hat{U}^\dagger \hat{h}_0 \hat{U} & \hat{S} &= \hat{U}^\dagger \hat{n} \hat{U} & \hat{D} &= \hat{W}^\dagger \hat{h}_1 \hat{W} \\ &= \mathrm{diag}(E_1, \ldots), & &= \mathrm{diag}\left(\left(1 + e^{\beta(E_1 - \mu)}\right)^{-1}, \ldots\right), & &= \mathrm{diag}(d_1, \ldots), \end{aligned}$$

where $\hat{U}$, $\hat{W}$, $E_1, \ldots$, and $d_1, \ldots$ are the eigenvectors and eigenvalues of $\hat{h}_0$ and $\hat{h}_1$, respectively, Equation 4 can be rewritten as

$$\begin{aligned} \nu(\tau) &= \det\left[\hat{\mathbb{I}} - \hat{S} + \hat{S} e^{i\hat{E}\tau} \hat{M} e^{-i\hat{D}\tau} \hat{M}^\dagger\right], \\ \hat{M} &= \hat{U}^\dagger \hat{W}. \end{aligned} \tag{5}$$

3 Method

Using Equation 1, Equation 2, and Equation 3, the energies of a 20×20 model with $t_X = t_Y \equiv t$ and $m = 0, t, \ldots, 5t$ were calculated and plotted (Figure 1a). The bulk and edge probabilities for each eigenstate were also calculated and compared to their corresponding eigenvalue (Figure 1b).

Using Equation 5, and setting $t_X = t_Y \equiv t = k_B = 1$ and $\omega_0 = 0$ for convenience, the decoherence was calculated for

- $L = 3, 5, \ldots, 27, 29$;
- $m = 1, 3$;
- $T = 10^{-4}, 10^{-3.5}, \ldots, 10^{0.5}, 10^1$;
- $\mu = 0$;
- corner, edge, and center impurity location;
- $\Delta = 10^{-4}, 10^{-3.5}, \ldots, 10^{0.5}, 10^1$;
- $\tau \in \left[0, \frac{20}{\Delta}\right]$.[a]

[a]This Δ-dependent time range was chosen as it was noticed that the frequency of the decoherence phase $\theta(\tau)$ had an approximately linear dependence on the coupling strength Δ, and so the final time was chosen to have an inversely proportional relationship to Δ, in order to plot meaningful graphs of $\theta(\tau)$. This poses a problem mainly when plotting with multiple values of Δ on a single plot, e.g Figure 5.

Using these calculated values, the decoherence magnitude $|\nu(\tau)|$ and phase $\theta(\tau)$ were plotted for each combination of these parameters, as well as $-\log_{10}(|\nu(\tau)|)$ on linear and logarithmic time axes.[b]

The estimate of the frequency f of the decoherence phase was also calculated for $L = 29$, $\mu = 0$, and all other parameters as above. This was carried out by locating the times τ_i at which $\theta(\tau_i) = 0$, calculating the length of time in between each of these, and taking the median of these times to be the phase period.[c]

4 Results

4.1 Topological Behaviour & Bulk/Edge States

From Figure 1a, the system exhibits topologically non-trivial behaviour for $m < 2t$ and trivial behaviour for $m > 2t$, for $t_X = t_Y \equiv t$.

From Figure 1b, the values that connect the energy bands for $m = t$ correspond to edge states, whereas the energy bands for $m = t, 3t$ correspond to bulk states.

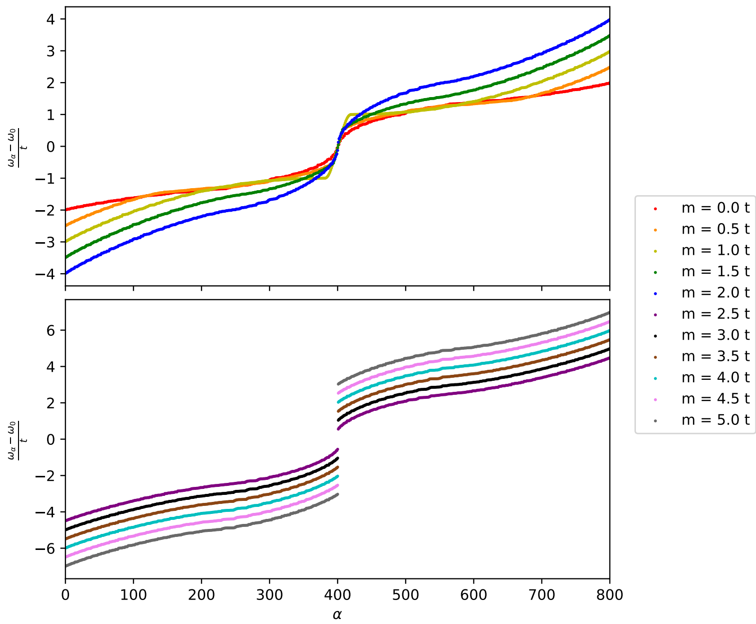

(a) Eigenvalues for $m = 0, t, \ldots, 5t$, split into the topologically non-trivial (top) and trivial (bottom) regimes.

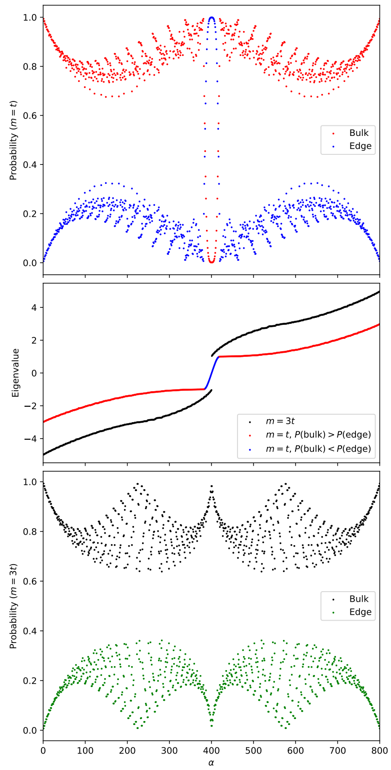

(b) Reproduction of Figure 1(c) from Mitchison et al. [2] (middle) showing eigenvalues for $m = t, 3t$, with extra plots (top & bottom) showing the corresponding bulk/edge state probability.

Figure 1: Energy eigenvalues of $\hat{h}_0$ for $L_x \times L_y = 20 \times 20$ and $t_X = t_Y \equiv t$.

[b]It was decided to also plot $-\log_{10}(|\nu(\tau)|)$ to help determine any possible relationships between the parameters.

[c]The median of these times was assumed to be the period as it was noticed that the phase oscillated very rapidly for certain parameters, e.g. Figure 6, and so there would be some times that corresponded to $\theta = 0$ but not to a full period.

4.2 Decoherence Magnitude

Energy Splitting The decoherence magnitude tended to decrease at a faster rate for $m = 1$ (topological insulator) than for $m = 3$ (trivial insulator) (Figure 2a), although the rates were more comparable at higher temperatures and coupling strengths (Figure 2b).

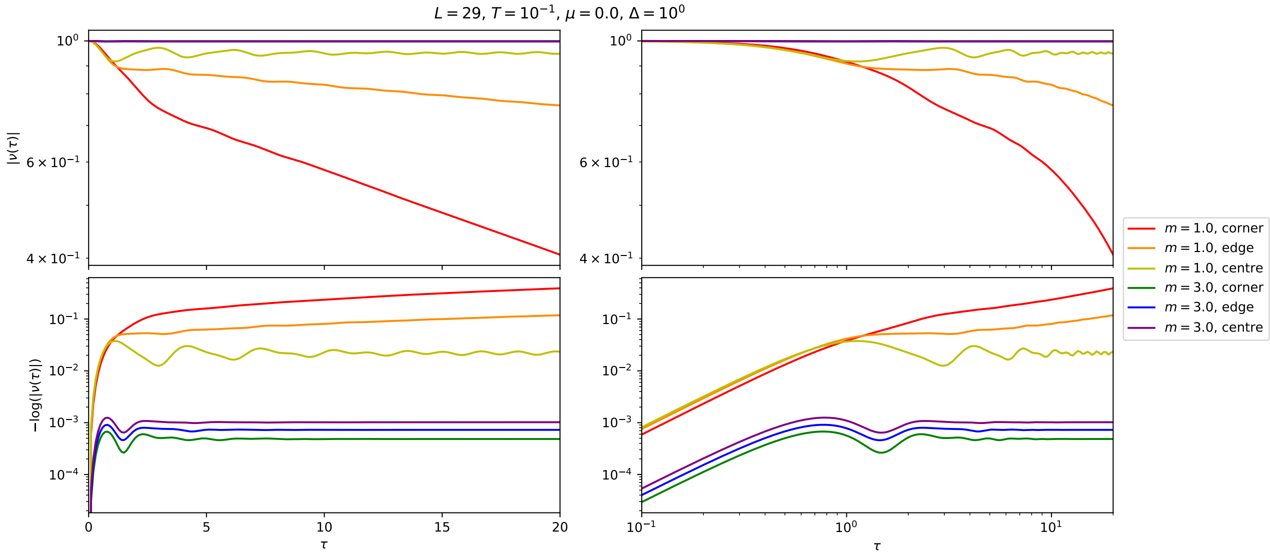

(a) $T = 0.1$, $\Delta = 1$.

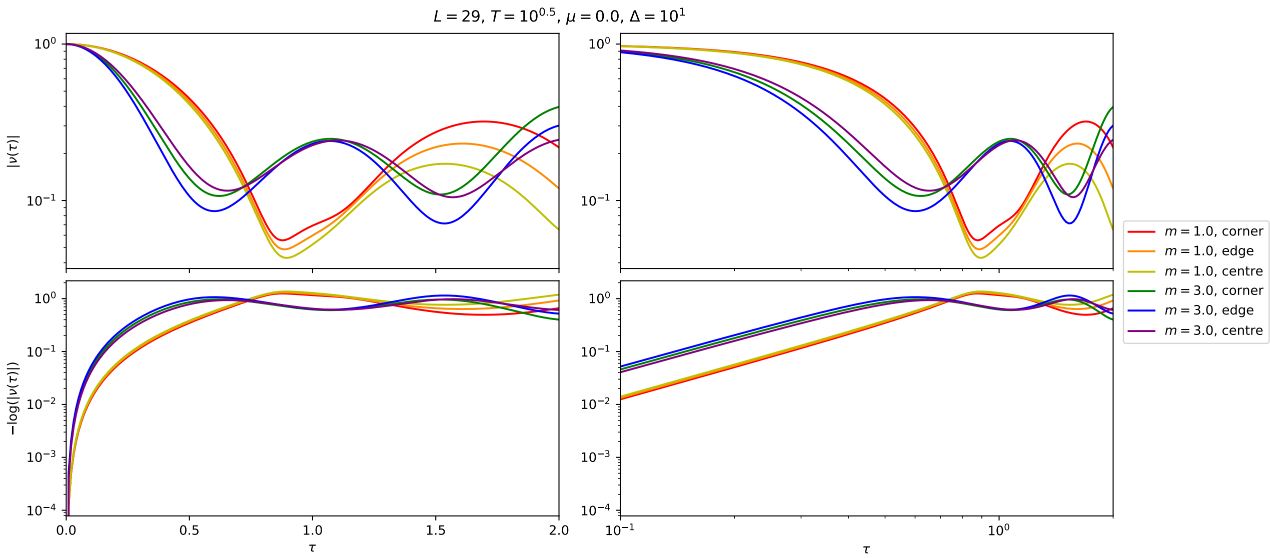

(b) $T = 10^{0.5}$, $\Delta = 10$.

Figure 2: Graphs of $|\nu(\tau)|$ (top) and $-\log_{10}(|\nu(\tau)|)$ (bottom) on linear (left) and logarithmic (right) time axes, for $L = 29$, $m = 1, 3$, $\mu = 0$, and corner, edge, and centre impurity location.

4.3 Decoherence Phase

4.3.1 Coupling Strength Proportionality

One of the most obvious relationships that was observed was the proportionality between decoherence phase frequency f and coupling strength Δ (Figure 3). For $L = 29$, $\mu = 0$, and $\Delta \leqslant 10^{0.5}$, it was found that $f \approx 0.15873\Delta$ (Figure 3a), with slight deviations occurring at $\Delta > 10^{-0.5}$ for $m = 1$ (Figure 3b) or $T > 10^{0.5}$ (Figure 3c).

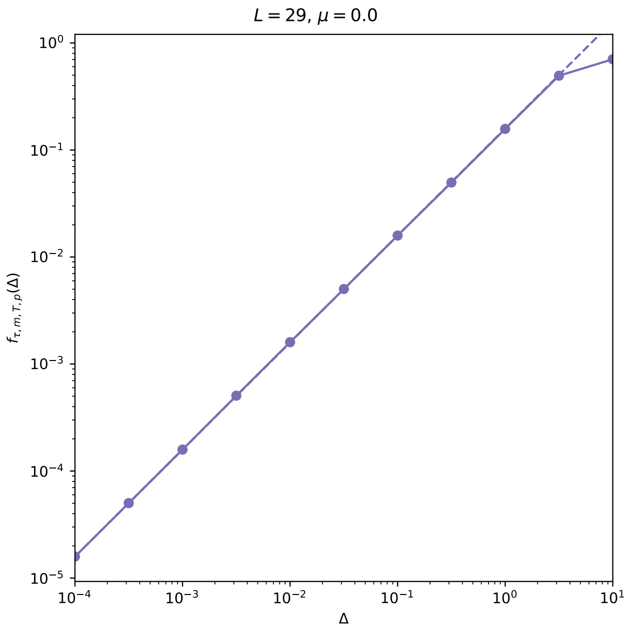

(a) Median over time τ, energy splitting m, temperature T, and impurity location p.

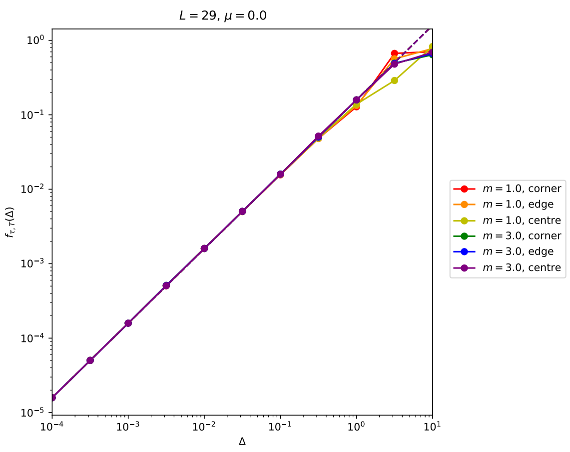

(b) Median over time τ and temperature T for $m = 1, 3$ and corner, edge, and centre impurity.

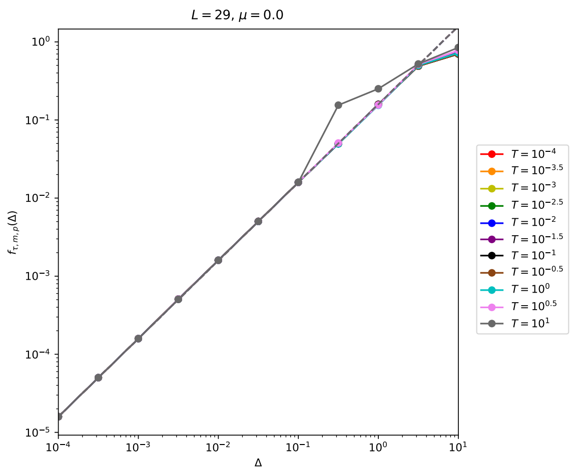

(c) Median over time τ, energy splitting m, and impurity location p for $T = 10^{-4}, \ldots, 10^{1}$.

Figure 3: Graphs of frequency f median against coupling strength Δ for $L = 29$ and $\mu = 0$. In each plot, the dashed line represents $f = 0.15873\Delta$.

4.3.2 Rate of Change

While for the largest system size considered in this project, i.e. $L = 29$, the rate of change of the decoherence phase θ was constantly negative (with some fluctuations for some parameter combinations), it was noticed for $L \leqslant 27$, $m = 3$, and $\Delta \geqslant 10^{-0.5}$ that certain parameter combinations resulted in a positive rate of change with a frequency not obeying the same proportionality law (Figure 4). The combinations of parameters that resulted in unexpected phase behaviour are detailed in Table 1.

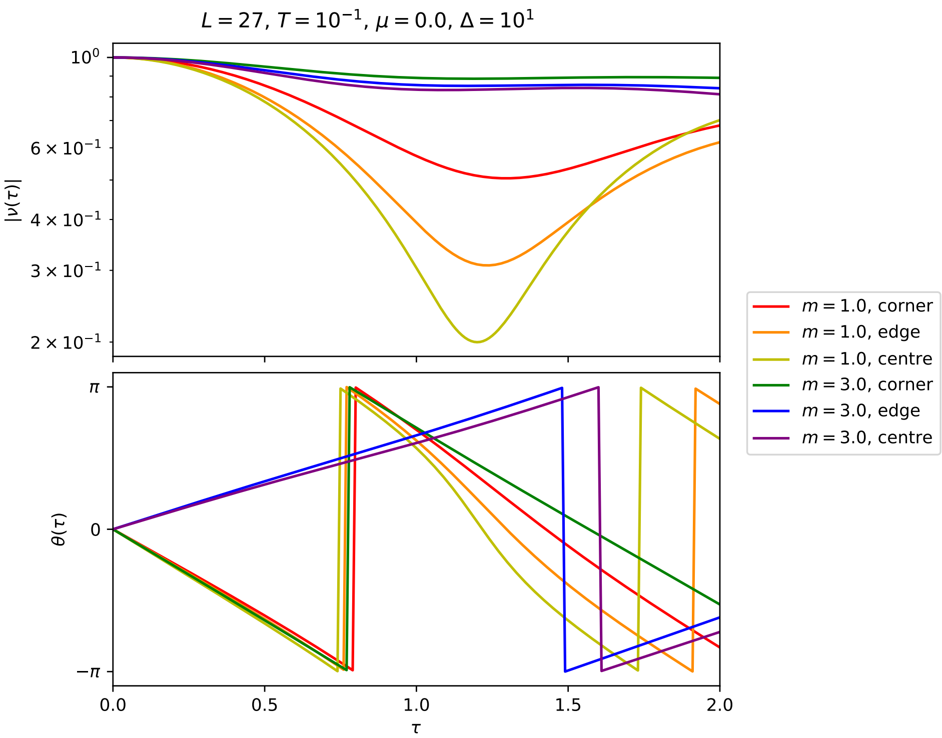

Figure 4: Graph of $|\nu(\tau)|$ (top) and $\theta(\tau)$ (bottom) for $L = 27$, $m = 1, 3$, $T = 0.1$, $\mu = 0$, corner, edge, and centre impurity location, and $\Delta = 10$. For $m = 3$ and edge and center impurity locations, the phase has a positive rate of change and a much smaller frequency than other combinations of m and impurity location.

<table>
<tr><th></th><th>$\Delta = 10^{-0.5}$</th><th>10^{0}</th><th>$10^{0.5}$</th><th>$\Delta = 10^{1}$</th></tr>
<tr><td>$L = 3$</td><td colspan="4">corner</td></tr>
<tr><td>5</td><td colspan="2">corner</td><td colspan="2">corner, edge</td></tr>
<tr><td>7</td><td></td><td>edge</td><td colspan="2">edge, centre</td></tr>
<tr><td>9</td><td></td><td colspan="3">corner, edge, centre</td></tr>
<tr><td>11</td><td></td><td></td><td></td><td></td></tr>
<tr><td>13</td><td></td><td></td><td></td><td></td></tr>
<tr><td>15</td><td colspan="2">corner</td><td colspan="2">corner, centre</td></tr>
<tr><td>17</td><td></td><td colspan="3">centre</td></tr>
<tr><td>19</td><td></td><td colspan="3">edge, centre</td></tr>
<tr><td>21</td><td></td><td colspan="3">corner</td></tr>
<tr><td>23</td><td></td><td>corner</td><td colspan="2">corner, edge</td></tr>
<tr><td>25</td><td>corner</td><td colspan="3">corner, edge</td></tr>
<tr><td>$L = 27$</td><td></td><td>centre</td><td colspan="2">edge, centre</td></tr>
</table>

Table 1: Values of L, Δ, and impurity location that resulted in unexpected phase behaviour for $m = 3$ and $\mu = 0$. Blank cells correspond to expected behaviour (i.e. negative rate of change following a similar proportionality law) for corner, edge, and centre impurity location.

5 References

[1] X. L. Qi, Y. S. Wu, and S. C. Zhang, "Topological quantization of the spin hall effect in two-dimensional paramagnetic semiconductors," *Physical Review B*, vol. 74, no. 8, 2006.

[2] M. T. Mitchison, A. Rivas, and M. A. Martin-Delgado, "Robust nonequilibrium edge currents with and without band topology," *Physical Review Letters*, vol. 128, no. 12, 2022.

[3] M. T. Mitchison, T. Fogarty, G. Guarnieri, S. Campbell, T. Busch, and J. Goold, "In situ thermometry of a cold fermi gas via dephasing impurities," *Physical Review Letters*, vol. 125, no. 8, 2020.

6 Appendix

The code and graphs produced for this project can be found here.

List of Figures

List of Tables

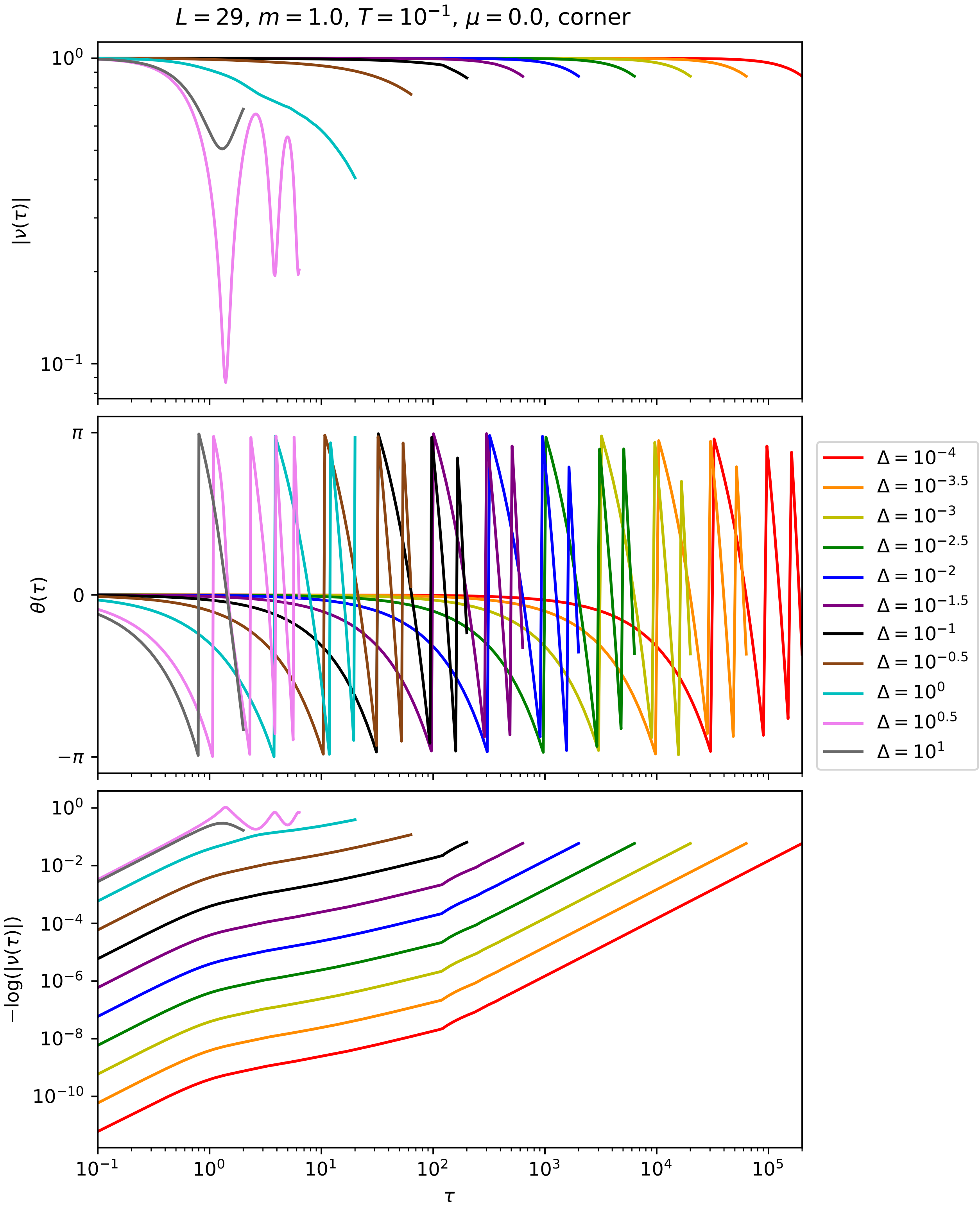

Figure 5: Graphs of $|\nu(\tau)|$ (top), $\theta(\tau)$ (middle), and $-\log_{10}(|\nu(\tau)|)$ (bottom) for $L = 29$, $m = 1$, $T = 0.1$, $\mu = 0$, corner impurity, and $\Delta = 10^{-4}, \ldots, 10^{1}$.

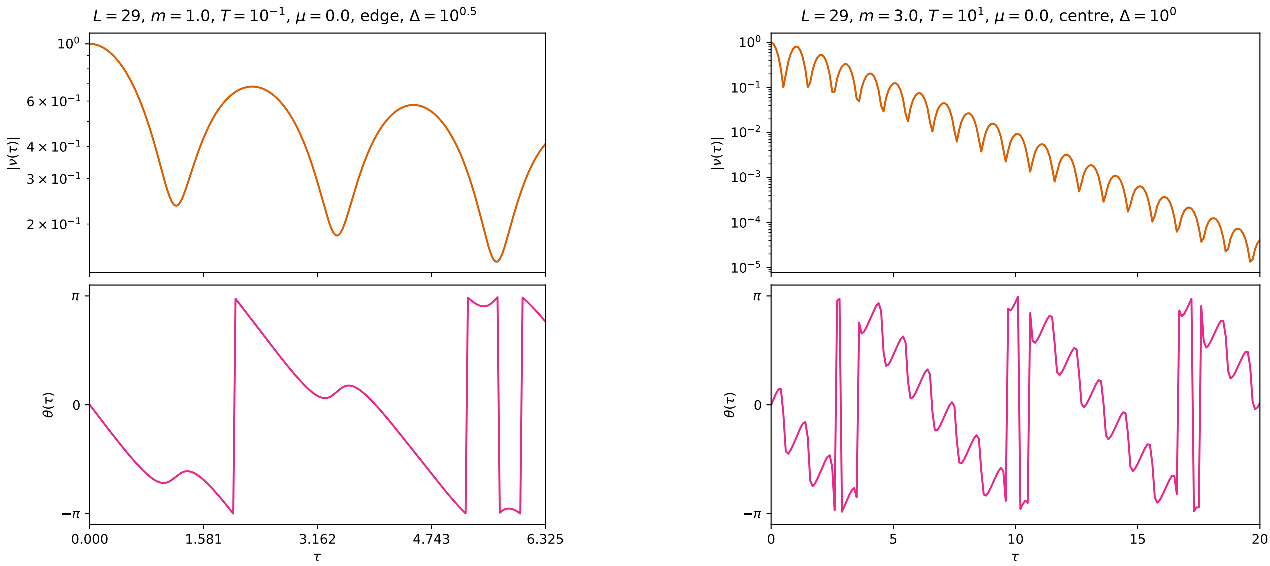

(a) $m = 1$, $T = 0.1$, edge impurity, $\Delta = 10^{0.5}$.

(b) $m = 3$, $T = 10$, centre impurity, $\Delta = 1$.

Figure 6: Graphs of $|\nu(\tau)|$ (top) and $\theta(\tau)$ (bottom) showing oscillatory behaviour for $L = 29$, $\mu = 0$.